1

Iron-Catalyzed Homogeneous Hydrogenation Reactions

Thomas Zell and Robert Langer

Philipps-University Marburg, Department of Chemistry, Hans-Meerwein-Straße, 35043 Marburg, Germany

1.1 Introduction

During the past decade, increasing attention has been drawn to iron-based catalysts as a substitute for ruthenium and other noble metal catalysts in homogeneous hydrogenation reactions. This is in part due to the fact that iron is more abundant, much less expensive, and it is also believed to be less toxic than are noble metals. Most importantly, nature uses 3d metals such as iron in highly active metalloenzymes like hydrogenases. However, nowadays, most reports, claiming to provide inexpensive and environmentally benign catalyst alternatives based on iron, often obviate the cost of the employed ligand(s) and usually provide no evidence for a reduced toxicity or the environmental sustainability of the reported iron complexes.

Moreover, iron-based catalysts are currently, in most cases, less active (lower TOF[1]) and exhibit lower productivities (lower TON[2]) than, for example, their ruthenium-based counterparts. While in the chemical industry, by scale hydrogenation reactions represent one of the biggest homogeneously catalyzed processes for the production of bulk chemicals, none of the current processes uses an iron-based catalyst. From an economic point of view, iron catalysts are obviously not yet sufficiently attractive to replace noble metal catalysts, indicating that still substantial improvements in catalyst development have to be made to achieve the goal of providing ***real*** alternatives to noble metal based catalyst systems for hydrogenation reactions. Nonetheless, the extremely high activity of hydrogenase enzymes as well as the activity of certain iron catalysts in different reactions involving hydrogen indicate the enormous potential of iron-based hydrogenation catalysts and may give rise to the assumption that this field of research will be a "hot topic" in the upcoming decades, too. This chapter intends to illustrate fundamental differences between iron and noble metal complexes that have to be considered in catalyst design, including fundamental

---

1 TOF = turnover frequency = $\frac{TON}{t}$.
2 TON = turnover number = $\frac{\text{mole of product}}{\text{mole of catalyst}}$.

coordination chemistry aspects as well as mechanistic considerations. Finally, for various substrates, state-of-the-art iron catalyst systems are compared.

At this point, it may be noted that the field of Fe-based hydrogenation catalysis is rather young, when compared to classic and well-established noble metal counterparts. Throughout the past decade, there was a significant synthetic progress in the development of synthetically valuable protocols for Fe-based hydrogenation reactions. In contrast, it turns out that often substantial mechanistic information is rather scarce. The fact that, in many cases, comprehensive analytic data is missing can in part be attributed to restrictions of spectroscopic methods and complications in the analysis of pressurized reactions. In addition, quantum chemical simulations are often more complicated than those for noble metal catalysis, simply due to the fact that more electronic configurations are energetically accessible, which is a result of lower ligand field splitting. Hence, for the calculations, high accuracy methods are required in order to assign the energetically most favored reaction pathways and possible decomposition pathways of active catalyst species.
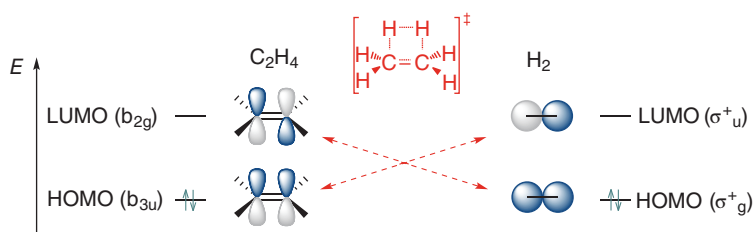

Figure 1.1 Schematic representation of LCAO-derived frontier orbitals of ethylene and H_2, illustrating that direct orbital interactions are forbidden by symmetry.

The direct concerted addition of H_2 to an unsaturated organic molecule is usually not favorable and exhibits too high reaction barriers, due to the lack of suitable frontier orbital interactions. Using the simplest example of ethylene and dihydrogen, Figure 1.1 visualizes that the two possible HOMO–LUMO combinations are forbidden by symmetry. Although the reaction of ethylene with dihydrogen to ethane is kinetically hindered by a high energetic barrier, from a thermodynamic point of view it is highly favorable; it is exergonic by $\Delta G = 101$ kJ/mol. For this reason, a catalyst is required to facilitate this thermodynamically favorable reaction by lowering the activation energies (Scheme 1.1).

The role of such a homogeneous hydrogenation catalyst can be reduced to two simple reaction steps (Scheme 1.1): (i) the activation of H_2 by heterolytic cleavage
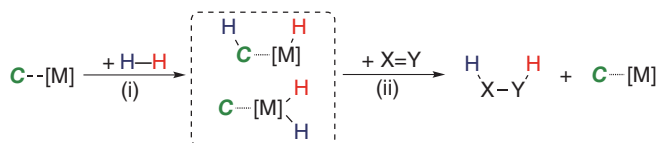
Scheme 1.1 Basic roles of homogeneous hydrogenation catalysts: H_2 activation (i) and transfer of the activated H_2 (ii). C indicates a functional ligand that can act as cooperative site).

or oxidative addition and (ii) the transfer of the activated H_2 to the substrate. While step (i) mainly depends on the type of ligand, the central metal atom and its formal oxidation state, the most viable mechanistic pathway of step (ii) strongly depends on the substrate and the polarity of the multiple bond that gets hydrogenated.[3]

1.2 Fundamental Differences Between Noble and 3d Metal Complexes

Common approaches in catalyst design with 3d metals either involve mimicking the reactivity of noble metal based analogs or circumventing undesired reactivity patterns, such as one-electron redox steps, by utilization of special ligands, such as *redox-active* ligands. For both strategies, it is of utmost importance to understand basic differences in physical and chemical properties and reactivity between 3d metals and noble metals. In the following sections, we focus on comparing properties of iron complexes with those of ruthenium complexes and in part with other noble metals (Table 1.1).

As geometric constraints of the utilized ligands strongly influence the catalyst activity, the difference in ionic radii deserves some attention. Comparing Shannon radii for the formal oxidation state +III, it becomes evident that low-spin iron(III) is significantly smaller than ruthenium(III), which exclusively appears in a low-spin configuration [1]. However, the Shannon radius of high-spin iron(III) is only slightly smaller than that of ruthenium(III). When aiming to mimic the reactivity of ruthenium complexes with iron catalysts, it is necessary to design systems which operate in low-spin configurations throughout the catalytic cycle. A significant difference of ionic radii should be taken into account, although

Table 1.1 Selected properties of iron, ruthenium, and their complexes.

	Fe	Ru
Ionic radii(pm)	55 (Fe^{III}, ls)[a] 64.5 (Fe^{III}, hs)[a]	68 (Ru^{III}, ls)[a]
$E°(M^{2+}/M^0)$ (V)	−0.44	+0.45
Occurrence of coordination numbers[b]	$6 > 5 \approx 4$	$6 \gg 5$
pK_a of $[L_nM(H_2)]$[c]	11.5	14.1

a) ls, low spin; hs, high spin.
b) Based on the number of entries in the CCDC database, reported in order of decreasing occurrence.
c) The pK_a values are reported for $[(dppe)M(H)(H_2)]^+$ (M = Fe, Ru; dppe = 1,2-bis(diphenylphosphino)ethane).

───────

3 It should be noted that, in principle, all the discussed mechanistic pathways can be realized for a certain substrate, but the most efficient catalysts usually operate via certain mechanisms, depending on the substrate and its polarity.

common polydentate ligands are usually sufficiently flexible to give stable complexes with both elements, Ru and Fe, in the same oxidation state.

As hydrogenation reactions occur naturally in reducing environments, a closer look at standard redox potentials reveals a second important difference. While ruthenium with a standard potential of $+0.45$ V for the Ru^{2+}/Ru^0 redox couple is a typical noble metal, the standard potential of iron for the Fe^{2+}/Fe^0 couple is only -0.44 V. In consequence, the reduction to ruthenium(0) would be expected to be a dominating deactivation pathway in catalytic hydrogenation reactions. This is, however, usually not observed. Based on the limited available mechanistic information, iron complexes rather get deactivated by reduction under hydrogenation conditions, demonstrating that the actual situation is more complex and influenced by a number of factors.

In contrast to noble metals, which preferably react via two-electron redox steps, iron shows a distinct preference for one-electron steps. Against common beliefs, these redox steps are, in most cases, of secondary importance for iron-catalyzed hydrogenation reactions. With the reducing environment of hydrogenation reactions, oxidation is usually not a conceivable activation pathway and reduction often simply leads to inactive iron(0) complexes or catalyst decomposition, e.g. by loss of ligands. Furthermore, for catalysts operating via a concerted mechanism, the formal oxidation state does not change within the catalytic cycle. In general, kinetic phenomena seem to outweigh thermodynamic properties in these reactions. A closer look at typical reaction steps involved in the catalytic hydrogenation of carbonyl compounds reveals that the change of spin multiplicity in reaction steps can be problematic and result in additional energetic barriers (Scheme 1.2).

The square planar and diamagnetic Vaska's complex with a d^8 electron count (Scheme 1.2a) shows a reactivity pattern, typical for noble metals. Coordination of H_2 results in a *penta*-coordinated diamagnetic intermediate that undergoes subsequent oxidative addition to a diamagnetic, octahedral dihydride complex. While no change of spin multiplicity is observed in this sequence, the situation changes for iron. From gas-phase studies it is known that $[Fe(CO)_4]$ (d^8 electron count) exhibits a distorted tetrahedral coordination geometry with a triplet ground state ($S = 1$), suggesting that the ligand field splitting of carbonyl ligands is too low for iron(0) to affect spin pairing and the stabilization of a square planar complex (Scheme 1.2b) [2]. Distorted tetrahedral coordination geometries are observed with phosphine ligands too, which are an important class of ligands in hydrogenation reactions for both iron and ruthenium. However, the coordination of a fifth carbonyl ligand to $[Fe(CO)_4]$ under formation of the *penta*-carbonyl complex $[Fe(CO)_5]$ or the oxidative addition of H_2 to give $[Fe(CO)_4(H)_2]$ results, in both cases, in diamagnetic complexes with a singlet ground state ($S = 0$). This change of spin multiplicity results in additional (spin-induced) barriers, which, in the current case, are observed for CO and H_2 coordination to $[Fe(CO)_4]$. This is in accordance with the observation of inverse kinetic isotope effects.

Ruthenium(II) complexes containing a cooperative ligand site are among the most active catalysts for the hydrogenation of carbonyl compounds. Similarly, the corresponding iron(II) complexes show impressive catalyst performances, too. In most cases, these catalysts share the same type of intermediates (Scheme 1.2c):
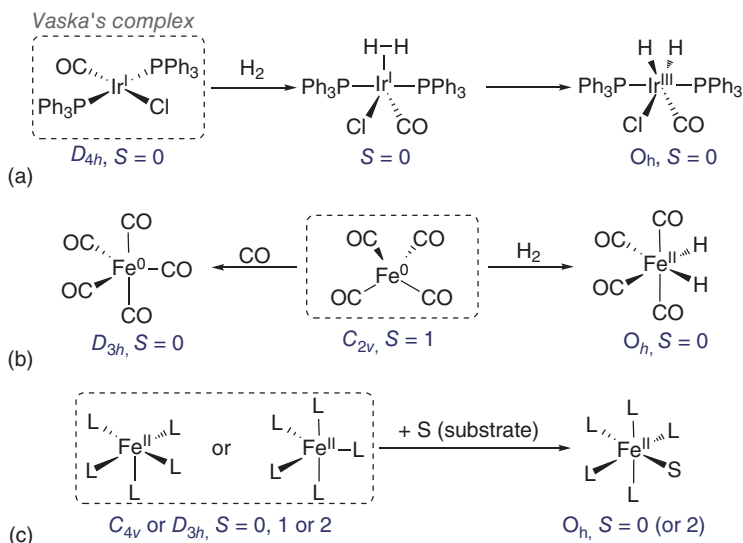
Scheme 1.2 (a) Oxidative addition without change of spin multiplicity, typical for noble metals. (b) Oxidative addition and ligand coordination to [Fe(CO)$_4$], which is associated with a change of spin multiplicity. (c) Possible spin multiplicities for the coordination of substrate (e.g. H$_2$) to a *penta*-coordinated d^6 metal fragment.

a *penta*-coordinated intermediate that allows for H$_2$ coordination prior to heterolytic H—H bond cleavage. The resulting hydride complex facilitates the proton–hydride transfer, regenerating the *penta*-coordinated intermediate. The latter species can exhibit square pyramidal (C_{4v}) or a trigonal bipyramidal geometry (D_{3h}). Depending on the metal and the utilized ligands, singlet ($S = 0$), triplet ($S = 1$), and quintet ($S = 2$) ground states can by realized. The additional hydrido ligand usually gives rise to a very strong ligand field in the corresponding octahedral complexes, so that a singlet ground state is commonly observed. In consequence, spin-induced barriers are avoided only if the *penta*-coordinated intermediates are diamagnetic, too. For ruthenium(II), these *penta*-coordinated intermediates are exclusively diamagnetic, but for iron, this strongly depends on the ligand environment. An alternative scenario involves solvent coordination and formation of an octahedral, diamagnetic intermediate, which, in principle, can react via an interchange mechanism with H$_2$ to give the octahedral hydride complex.

For example, the square pyramidal complex **1** is diamagnetic and one of the most active catalysts for the transfer hydrogenation of ketones to alcohols using isopropanol as hydrogen source (Figure 1.2) [3]. Its reaction with isopropanol yields the corresponding octahedral and diamagnetic hydrido complex, which is the active reducing species. The square pyramidal amido iron complex **2** is diamagnetic as well and the most active iron catalyst known to date for the hydrogenation of carbonyl and carboxyl compounds to alcohols [4]. The coordination of H$_2$ and its subsequent heterolytic cleavage across the Fe—N bond yields the active dihydride species. The diamagnetic and trigonal bipyramidal complex **3**
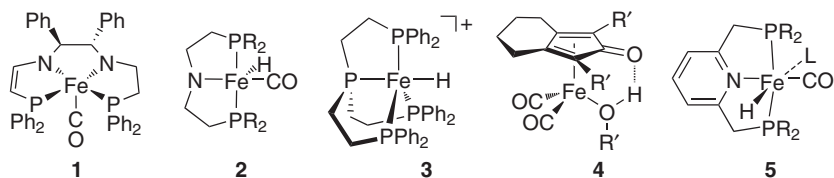
Figure 1.2 Detectable or isolable, *penta*-coordinated or solvent coordinated intermediates with a singlet ground state (R = *i*-Pr; R′ = SiMe$_3$).

is an active catalyst for the hydrogenation of carbon dioxide [5]. The coordination of CO$_2$ in *cis* position to the hydrido ligand leads as well to an octahedral intermediate with $S = 0$.

The hypothesis that highly active iron catalysts for the hydrogenation of carbonyl compounds avoid a change of spin state within the catalytic cycle is provided by the observation of different solvent coordinated complexes, such as **4** [6] and **5** [7], which therewith avoid the formation of potentially paramagnetic, *penta*-coordinated intermediates by associative or interchange substitution mechanisms. However, for olefins and other nonpolar substrates, high-spin complexes are frequently employed as catalysts, and they also were identified in many cases as intermediates in catalytic reactions. The participation of different spin surfaces has been demonstrated for elementary steps of iron complexes in the gas phase and is currently discussed as a viable mechanistic scenario for these catalysts [8]. The next paragraphs discusses the aspect that this violation of the spin conservation paradigm is related to a stepwise mechanism.

Further important points, when it comes to catalyst design, are the coordination number and the number of donor groups in the employed ligand (denticity). An analysis of the occurrence of certain coordination numbers for iron and ruthenium in the Cambridge Crystallographic Data Centre (CCDC) revealed that both metals have a preference for the coordination number 6, while 5 is common for both metals as well.[4] Most interestingly, tetra-coordinated iron complexes are very common as well, but in the case of ruthenium, the coordination number 4 is rare and can only be observed when bulky polydentate ligands are employed. It is well known that in a weak ligand field, iron(II) easily forms tetrahedral complexes, which are usually catalytically inactive. These findings have important consequences for the type of ligand used in iron catalysts: while mono- and bidentate spectator ligands allow for the formation of tetrahedral deactivation products (e.g. by dissociation of one ligand), these pathways can partially be suppressed when using tri- and tetradentate ligands.

The catalytic hydrogenation of carbonyl compounds involves the transfer of a hydrido ligand to the carbonyl carbon atom. The hydride donor ability of metal hydrido complexes can be quantified by the so-called hydricity, which represents the Gibbs enthalpy ($\Delta G^{\circ}_{H^-}$) for Eq. (1.1), the heterolytic cleavage of the M—H bond to a hydride and a corresponding metal fragment. Although experimental data on hydricity of iron(II) and ruthenium(II) complexes is limited, it becomes

---

4 The discussed results are based on a CCDC database search for iron and ruthenium complexes with different coordination numbers in August 2016.

evident that the hydride donor ability of iron complexes is significantly lower than that of ruthenium complexes [9].

$$[L_nM(H)] \rightarrow [L_nM]^+ + H^- \ (\Delta G_{H^-}^{\circ} > 0) \tag{1.1}$$
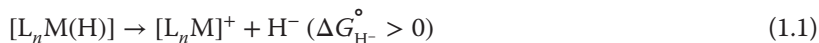
For catalysts that activate H_2 by heterolytic cleavage, the acidity of the corresponding dihydrogen complexes is an essential property. These heterolytic cleavage processes can, in other words, also be regarded as deprotonation reactions of the dihydrogen complexes with an internal or external base. Available experimental data that allows a direct comparison between iron and ruthenium dihydrogen complexes is limited, but the pK_a values of complexes with the general formulae $[(dppe)_2M(H)(H_2)]^+$ (M = Fe, Ru; dppe = 1,2-bis(diphenylphosphino)ethan) indicate that the iron dihydrogen complex is even more acidic ($pK_a = 11.5$) than the corresponding ruthenium complex ($pK_a = 14.1$) [10]. However, using an increment system developed by Morris, the estimated pK_a values for different relevant dihydrogen complexes are identical, which indicates that the heterolytic cleavage of dihydrogen is not problematic for iron catalysts [10b].

Easy accessible deactivation pathways can drastically limit the catalytic productivity and possible catalyst loading, but detailed information on catalyst deactivation steps is often missing. However, the formation of (ligand protected) nanoparticles that remain catalytically active has, in some cases, been reported as well as the detection of well-defined inactive iron(0) complexes. Pincer-type complexes with one ancillary carbonyl ligand (Scheme 1.3) serve as an illustrative example. This type of compounds represents a class of highly active hydrogenation catalysts for both metals, iron and ruthenium. The active species **6** gets presumably deactivated by reduction to the tetra-coordinated complex **7**, which for ruthenium is square planar ($S = 0$) and can exhibit a distorted tetrahedral environment in case of iron ($S = 1$). In consequence, de- and reactivation of iron complexes are associated with additional (spin-induced) barriers, which might cause irreversibility of this deactivation pathway in many cases. Based on the standard potential, the formation of ruthenium metal should be facile, but, as pointed out earlier, the formation of tetra-coordinated ruthenium complexes is not favored for ruthenium complexes and the absence of spin-induced barriers allows for fast reactivation. For this type of iron catalysts, the formation of *penta*-coordinated iron(0) complexes **9** together with equimolar amounts of the uncoordinated ligand **8** were observed in several cases [7b, 11].
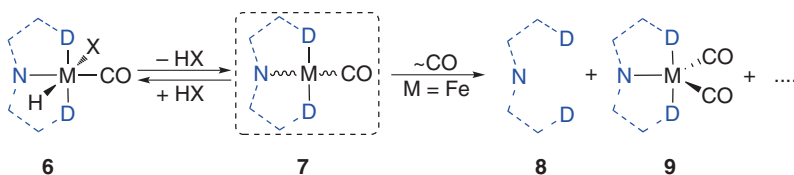
Scheme 1.3 Observed decomposition pathway of iron and ruthenium pincer-type complexes with an ancillary carbonyl ligand via the proposed intermediate **7** (M = Fe, Ru; D = donor group; X = H, alkoxide).

For nonrigid tetradentate ligands, similar observations were made: the catalytically inactive complex $[(\kappa^4\text{-PNNP})Fe(CO)]$ is formed during the catalytic

reaction (PNNP $= $ Ph$_2$P—C$_6$H$_4$—CH=N—CH$_2$CH$_2$—N=CH—C$_6$H$_4$—PPh$_2$). Interestingly, this complex was demonstrated to serve as a source for catalytically active iron nanoparticles [12].

In view of the standard potentials for the M^{2+}/M^0 couple, the observed deactivation pathways appear counterintuitive, but might be rationalized by the preference for different coordination numbers as well as different spin states of intermediates of iron and ruthenium catalyst systems.

1.3 Mechanistic Scenarios and the Role of Substrates

The apparent dependence of the mechanism of the hydrogen transfer step on the substrate polarity mainly originates from a preference for a certain coordination mode of each substrate: nonpolar substrates such as olefins coordinate in a side-on manner to the central metal atom, which makes a migratory insertion of the side-on coordinated substrate into the M—H bond viable. Polar substrates are often end-on coordinated to the central metal atom, which slows down the migratory insertion step, and a concerted proton–hydride transfer from the catalyst to substrate is usually faster. However, for carbon dioxide and for nitriles, for example, evidence has been provided that both stepwise migratory insertion mechanisms and concerted proton–hydride transfer can occur efficiently depending on the nature of the catalysts. In the following paragraphs, we discuss the available mechanistic information for iron-based catalysts in the context of the most common mechanisms for the hydrogenation of polar and nonpolar substrates. For relevant examples, the mechanistic information is compared to noble metal based catalysts.

1.3.1 Nonpolar Substrates

Iron-catalyzed hydrogenation reactions of olefins and alkynes have been known for several decades and usually proceed via mechanisms in which the hydrogen is transferred in a stepwise manner [13]. For well-established homogeneous noble metal hydrogenation based on rhodium and iridium, two types of textbook mechanisms are known [14]. The difference between these mechanisms is the order of the three basic steps involved in the stepwise hydrogen transfer: oxidative addition of H$_2$, migratory insertion in the M—H bond, and C—H reductive elimination of the product (Scheme 1.4). Cycle **A** involves a monohydride as active species that allows for the side-on coordination of the unsaturated substrate in *cis* position to the hydrido ligand. Migratory insertion leads to an alkyl complex. The subsequent reaction of this intermediate with H$_2$ results in product release and regeneration of the active monohydride. As the H$_2$ activation and product release do not necessarily involve a change in the formal oxidation state, this is a common mechanism for d^6 metal catalysts. A typical example would be ruthenium(II)-based catalysts. The second cycle (**B**) includes oxidative addition of H$_2$ and coordination of olefin to a metal complex [M]. Notably, the order can vary; in Scheme 1.4, for simplicity, only one case is depicted. The resulting dihydride olefin species allows for migratory insertion of the olefin into the metal
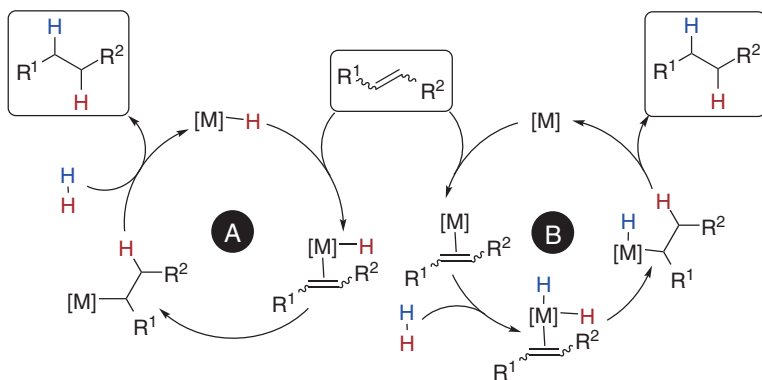
Scheme 1.4 Simplified reaction mechanisms for the hydrogenation of C—C multiple bonds, depicted for olefins.

hydrogen bond. Subsequently, reductive C–H elimination results in the release of the alkane product along with the initial catalyst species [M]. This mechanistic pathway is often assumed for homogeneous catalysts with a d^8 electron count (e.g. Rh^I, Ir^I). During the catalytic cycle, the change in oxidation states of the catalytic intermediates is by ± 2 (e.g. Rh^I/Rh^{III} and Ir^I/Ir^{III}).

One of the first well-defined iron-based hydrogenation catalysts, whose mode of action has been investigated, is the iron(II) complex $[(PP_3)Fe(H)(H_2)](BPh_4)$ (**10**, $PP_3 = P(CH_2CH_2PPh_2)_3$ Figure 1.3). It was employed as a catalyst for semihydrogenation of alkynes to alkenes [13]. The octahedral arrangement of the four phosphine donor group, one hydrido and one dihydrogen ligand results in a strong ligand field and, as a result, in a diamagnetic complex. Interestingly, the absence of a potentially cooperative ligand site indicates that this is not an essential requirement for this catalytic reaction. Kinetic studies on this system point toward a mechanism via cycle **A**, in which the coordination of the dihydrogen ligand seems to be rate determining.

The employment of the so-called *non-innocent* or *redox-active* ligands [15] in iron catalysts for olefin hydrogenation leads to a significant improvement of catalyst activity. One of the first examples is the iron complex $[(^{iPr}PDI)Fe(N_2)_2]$ (**11**) that contains the 2,6-di-*iso*-propylphenyl-substituted bis(imino)pyridine (^{iPr}PDI)
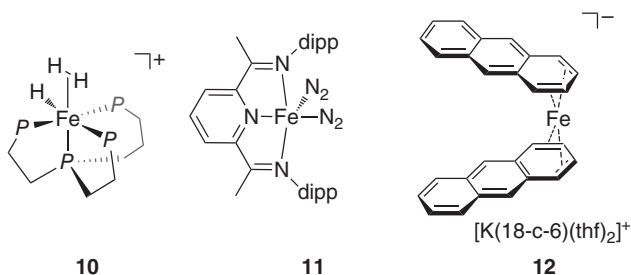

Figure 1.3 Examples of different types of iron catalysts for the hydrogenation C—C multiple bonds.

as non-innocent ligand [16]. Complex **11** efficiently catalyzes the hydrogenation of olefines to alkanes under mild conditions [16a]. Later on, it was shown that this type of hydrogenation can also be conducted for substrates containing functional groups with heteroatoms [17]. Initially, a mechanism proceeding via cycle **B** was suggested after dissociation of N_2 from **11**. Comprehensive mechanistic investigations indicate that for some complexes and catalytic intermediates, reversible reduction of the bisiminopyridine ligand takes place rather than reduction of the central iron atom.

Active iron catalysts for the hydrogenation of olefins can also be formed by the reaction of $FeCl_3$ and $LiAlH_4$ in the presence of suitable arenes [18]. Under reaction conditions, it is assumed that bisligated iron(0) complexes are formed, which allows for olefin coordination and H_2 activation. Notably, the nature of the active catalyst changes during the reaction from a homogeneous system to a heterogeneous, but still active, system. The ferrate complex **12** (Figure 1.3) is an active olefin hydrogenation catalyst as well [19]. Here, the exchange of one arene ligand by an olefin generates the catalytically active species, which subsequently activates H_2. Mechanistic investigations point toward the mechanism shown in cycle **B**.

These examples clearly illustrate that catalytic activity in olefin hydrogenation can be achieved with a variety of iron catalysts, ranging from well-defined non-functionalized catalysts to complexes with non-innocent ligands, nanoparticles, and poorly defined, and also *in situ* generated catalysts. Based on the current mechanistic understanding, it can be concluded that it is not necessary to mimic the conventional reactivity patterns of noble metal catalysts to achieve catalytic activity with iron complexes. Moreover, in some cases, the tendency of 3d medals to undergo one-electron redox steps seems even advantageous.

1.3.2 Polar Substrates

For hydrogenation reactions of polar bonds, completely different reactivity patterns and mechanisms are observed. For many catalysts, a stepwise mechanism via migratory insertion of a polar multiple bond into a metal hydrogen bond was demonstrated to be inefficient. It has been reasoned that polar substrates such as carbonyl compounds preferably coordinate in an *end-on* κO manner to the metal and not a *side-on* manner like apolar substrates such as olefins or alkynes. The migratory insertion of such *end-on* coordinated substrates is often disfavored, due to too high reaction barriers [20]. In the case of simple ruthenium phosphine complexes, it was shown that addition of a chelating primary amine ligand accelerates the rate of ketone hydrogenation by orders of magnitude. The resulting catalytically active species is often called a bifunctional or cooperative catalyst [21], which is based on the finding that the coordinated amine ligand can act as a proton source in a concerted proton–hydride transfer from the catalyst to the polar substrate (cycle **C** in Scheme 1.5). This *in concerto* mode of action is also called metal ligand cooperation. Although, ruthenium complexes with different ligand platforms and functionalities can be active hydrogenation catalysts, which, in principle, can follow different mechanisms, cooperative catalysts turned out to be particularly active catalysts for the hydrogenation of polar multiple bonds.
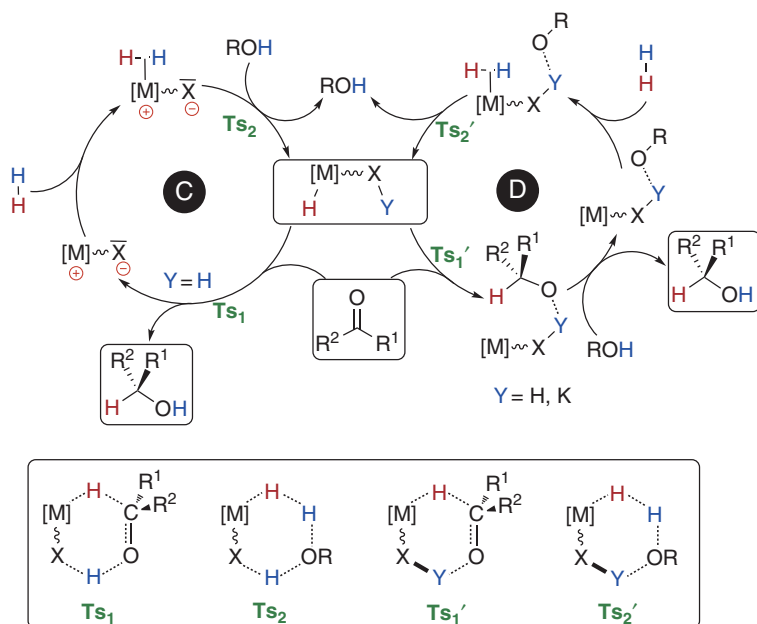
Scheme 1.5 Simplified reaction mechanisms for the hydrogenation of C—O multiple bonds, depicted for olefins.

It is worth noting that the mechanistic view of a concerted proton–hydride transfer (as in **TS₁**) was recently questioned by DFT studies with explicit solvent modeling [22]. It was suggested that for a number of catalysts the cooperative site serves as a binding site for the substrate that allows for pre-coordination of the substrate and the subsequent hydride transfer (**TS₁′**). It has been further indicated that a potassium ion (in many cases, the counterions of the utilized base) can also be involved in this interaction (cycle **D**). The H···O- or K···O-bound alkoxide either serves as the internal base in the heterolytic cleavage of dihydrogen or is protonated and exchanged by the alcohol solvent prior to dihydrogen cleavage.

A closer look at the reported iron catalysts for the hydrogenation of polar multiple bonds reveals that the most active catalysts contain cooperative ligands and that they usually operate via the simplified mechanism shown in Scheme 1.5.

1.3.3 Exceptions

In the previous paragraphs, we have summarized the available mechanistic information on the operating mechanisms of the most active catalysts. The conclusion from this information might be taken as a rule of thumb for the prediction of a viable mechanism and catalyst design, but there are many exceptions and these are briefly discussed in following paragraphs.

Carbon dioxide is readily hydrogenated to formates in the presence of stoichiometric amounts of a base and a suitable catalyst. Despite the polar C—O bond,

highly active catalysts were reported with cooperative and noncooperative ligands, operating via different mechanisms [23]. It has even been demonstrated that ruthenium catalysts facilitating an inner-sphere mechanism allow for the direct hydrogenation to methanol [24].

A recent study suggested that an amine-based iron pincer catalyst for the hydrogenation of olefins operates via a stepwise cooperative mechanism [25]. For this catalyst system, this might be the preferred pathway, as the active reducing dihydride species does not have any vacant coordination site, allowing for olefin coordination.

Nitriles are common ligands in coordination chemistry and, like ketones, they usually prefer an *end-on* coordination. Although some cooperative ruthenium catalysts are known to operate via the mechanisms shown in Scheme 1.5 [26], it has also been demonstrated for a pyridine-based ruthenium pincer catalyst that the reaction can proceed via an intermediate with a *side-on* coordinated nitrile and a subsequent migratory insertion [27].

1.4 Iron-Catalyzed Hydrogenation of C—C Multiple Bonds

In the Section 1.3.1, highly active iron catalysts for the hydrogenation of C—C multiple bonds were introduced. The following Sections 1.4.1 and 1.4.2 discusses the most active homogeneous iron-based catalysts for different transformations involving the hydrogenation of C—C multiple bonds, namely, the hydrogenation of olefins and alkynes.

1.4.1 Hydrogenation of Olefins

The hydrogenation of olefins (alkenes) to alkanes is catalyzed by a wide range of well-defined and *in situ* generated iron catalysts. Among the well-defined iron catalysts are complexes with potentially cooperative ligands that either act as internal base, sometimes described as a proton relay (e.g. the amido group in **13** [25] and **14** [28]), or as a hydride acceptor (e.g. the Z-type BR_3-group in **15** [29] (Figure 1.4)), as well as complexes with non-innocent (= redox active) ligands (**11** [16a]), formally an electron relay, or non-functionalized ligands (**12** [19]).

Also, *in situ* generated catalysts, such as the $FeCl_3/LiAlH_4$ system [18], can lead to highly active catalysts in terms of turnover frequency. However, the active species in these systems seem to have a limited lifetime, which is also reflected by the steady transition of a homogeneous to a heterogeneous catalyst system.

A comparison of the different catalyst types reveals that the pincer-type complex **11,** featuring the redox-active bis(imino)pyridine ligand, is by far the most active catalyst for the hydrogenation of mono- and disubstituted olefins (Table 1.2). However, substrates with tri- and tetrasubstituted C-C double bonds are not hydrogenated under the reported conditions [16a]. The *in situ* generated catalyst based on $Fe(hmds)_2/i$-Bu_2AlH, in contrast, appears to be less active for the hydrogenation of monosubstituted olefins, but is capable of hydrogenating

Figure 1.4 Representative examples of iron catalysts for the hydrogenation of olefins (in addition to the examples in Figure 1.3).
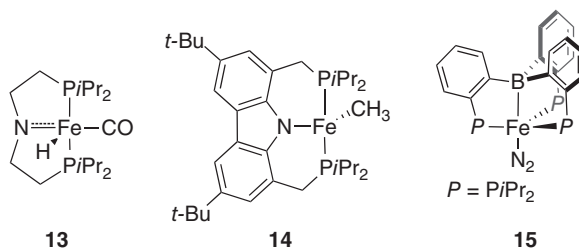

13   **14**   **15**

Table 1.2 Comparison of different catalysts for the hydrogenation of styrene.

Ph⌒ + H₂ —[Fe]→ Ph⌒

[Fe]	Loading (mol%)	$p(H_2)$ (bar)	Yield (%)	TON	TOF (h^{-1})	References
11	0.3	1	>99	330	1344	[16a]
12	1.0	2	95	95	32	[19]
13	5.0	1	>99	20	1	[25]
14	1.0	8	>99	100	17	[28]
15	3.3	1	95	29	0.27	[29]
$Fe(hmds)_2/i\text{-}Bu_2AlH^{a)}$	5.0	2	>99	20	6.67	[18]
$FeCl_3/LiAlH_4$	5.0	1	>99	20	3.33	[18]

a) Data is for *para*-butyloxystyrene.

tri- and tetrasubstituted olefines [18]. The diverse types of active catalysts again justify the conclusion that there are no specific catalyst requirements to achieve high activity in olefin hydrogenation.

1.4.2 Hydrogenation of Alkynes

The hydrogenation of alkynes can lead to different reaction products, depending on the type of catalyst and the reaction conditions. In general, the first hydrogenation step yields olefins, which, in the case of internal alkynes as substrates, can result in *E*- and *Z*-isomers (Scheme 1.6). As pointed out in the Section 1.4.1, olefins can get hydrogenated in the presence of a suitable catalyst as well, leading to saturated alkanes. If the main hydrogenation product(s) are olefins, the reaction is commonly called a semihydrogenation, as the main hydrogenation product remains unsaturated and does not get further hydrogenated (Scheme 1.6).
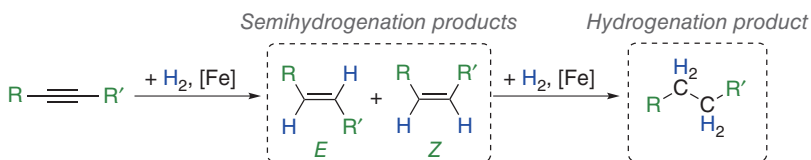
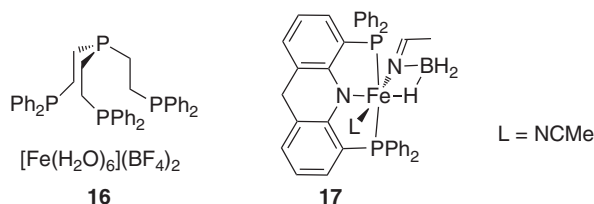**Scheme 1.6** Semihydrogenation and hydrogenation of alkynes.

L = NCMe

16   **17**

As for olefins, the examples of iron-based catalysts for the (semi)hydrogenation of alkynes are limited and often catalysts for the olefin hydrogenation are active for alkynes as well. The bisiminopyridine complex **11**, for example, is an active catalyst for the hydrogenation diphenylacetylene, too, which leads to the formation of *Z*-stilbene as an intermediate that gets further hydrogenated to dibenzyl over the course of the reaction [16a]. The selective formation of terminal olefins by semi-transfer hydrogenation of alkynes is catalyzed by an *in situ* generated catalyst (**16**), containing the tretraphos ligand and $[Fe(H_2O)_6](BF_4)_2$ (Figure 1.5) [30]. The highly desirable *E*-selective hydrogenation of internal alkynes is facilitated by the iron pincer catalyst **17** [31].

1.5 Iron-Catalyzed Hydrogenation of C—O Multiple Bonds

Organic carbonyl compounds containing a C=O double bond can exhibit distinct differences in their reactivity, as the substrate scope ranges from reactive aldehydes to inert substrates which are ureas, carbamates, and carbonates. The latter ones are sometimes even used as inert solvents for hydrogenation reactions [32]. Figure 1.6 illustrates the decreasing carbonyl reactivity of different selected substrates, with which it becomes more challenging to achieve a catalytic hydrogenation. Recently, significant progress has been made in the development of ruthenium catalysts that are capable of hydrogenating even the most inert substrates among these series, such as carbonates, carbamates, and ureas [32, 33]. With corresponding iron complexes, tremendous achievements in hydrogenation catalysis have been reported as well, but so far the hydrogenation activity has been limited to esters and even amides, as well as more reactive carbonyl compounds (Figure 1.6). These findings might be the result of reduced hydricity observed for iron complexes in comparison to the corresponding ruthenium analogs.
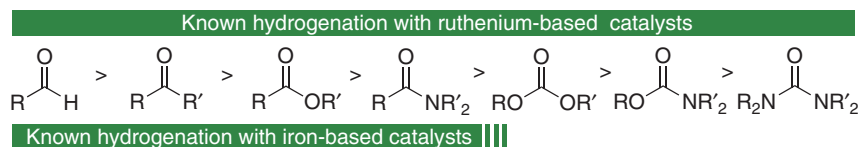

Figure 1.6 General reactivity of selected carbonyl compounds toward nucleophiles and the current state of research for the hydrogenation with iron and ruthenium catalysts.
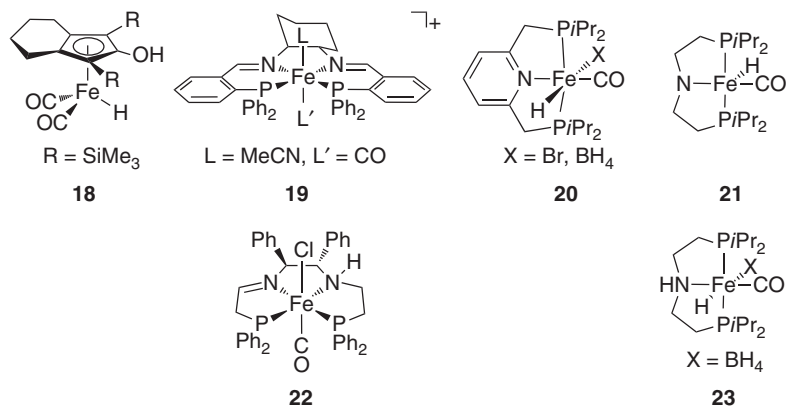
Figure 1.7 Selection of iron catalysts for the hydrogenation of aldehydes and ketones.

Typical, iron-based hydrogenation catalysts for carbonyl and carboxyl compounds are shown in Figure 1.7. For the majority of these catalysts, the underlying construction principles can be summarized as follows: (i) Cooperative ligands, acting as a proton relay, are found in the most active representatives. (ii) At least one polydentate or cyclopentadienyl ligand is present in these complexes. (iii) Donor groups and ligands with a strong field are employed in these ligands. In the following Subsections 1.5.1–1.5.3, we briefly discuss the recent developments and state-of-the-art iron catalysts for each substrate.

1.5.1 Hydrogenation of Aldehydes and Ketones

An important milestone in the development of iron-based hydrogenation catalysts was *Casey*'s report about the catalytic activity of *Knölker*'s complex **18** in the hydrogenation of aldehydes, ketones, and aldimines under mild conditions (3 bar H$_2$ pressure, rt) [34] (Table 1.3). Although the catalyst loading was quite high (2 mol%) and the yield of 1-phenylethanol was only 83%, it represented the first example of an iron-catalyzed ketone hydrogenation using hydrogen gas. While *in situ* generated transfer hydrogenation catalysts based on iron were reported early, the report of complex **19** as an efficient and enantioselective hydrogenation catalyst for ketones and imines represents an important breakthrough [11b]. The subsequent modification of the employed tetra dentate ligand in the past decade has led to chiral state-of-the-art catalysts for asymmetric transfer hydrogenation reactions, such as **22**, which exhibit in comparable activities and selectivity like noble metal catalysts [35].

The pyridine-based iron pincer complex **20** showed by an order of magnitude higher productivities TON and activities TOF in the hydrogenation of ketones with hydrogen gas (4.1 bar) [36]. Later on, complex **20** and related iron PNP-pincer (pre)catalysts based on pyridine backbones [36], were also employed as hydrogenation catalysts for other polar substrates including aldehydes [37], activated esters [38], and even amides [39]. Also, the efficient dehydrogenation of formic acid in the presence of amine additives was reported using iron

Table 1.3 Comparison of different catalysts for the hydrogenation of acetophenone.

			O		OH	
			Ph⋮⋮ + H$_2$ $\xrightarrow{\text{[Fe]}}$ Ph⋮⋮			
[Fe]	**Loading (mol%)**	**H$_2$ source**	**Yield (%)**	**TON**	**TOF (h^{-1})**	**References**
18	2.0	H$_2$ (3 bar)	83	42	2	[34]
19	0.25	*i*-PrOH	91	362	907	[11b]
20	0.05	H$_2$ (4 bar)	94	1 720	430	[36]
22	0.016	*i*-PrOH	82	5 000	10 000	[35]
23	0.05	H$_2$ (5 bar)	>99	2 000	500	[4]

pyridine-PNP catalysts [40]. Similar iron pincer complexes (**21** and **23**) were reported later on. The design principle of combining a PNP-pincer ligand with an ancillary carbonyl ligand resulted in highly active and productive catalysts systems for PNP ligands with aliphatic and olefinic backbones. This catalyst family was then applied in hydrogenation and dehydrogenation reactions for a variety of substrates [41]. Applications for this type of (pre)catalysts include hydrogen liberation from formic acid [42] and from aqueous methanol solutions [43], hydrogenation of ketones [11b, 44], esters [42a, 45], and amides [11a, 46], the asymmetric hydrogenation of ketones and imines [11b], the hydrogenation of polarized C-C double bonds of substituted alkenes [25], and the reversible hydrogenation and dehydrogenation of N-heterocycles [47].

Complexes **19** and **22** are chiral and capable of catalyzing the enantioselective hydrogenation of prochiral ketones to chiral alcohols with high selectivity (Figure 1.7). After the initial report on the first iron-based catalyst (**19**) [48] for this reaction, the activity and selectivity have been significantly improved with the modified tetra dentate ligand platform in **22** [42b, 49]. For other non-chiral iron catalysts shown in Figure 1.7, different strategies have been used for the introduction of a center of chirality in the catalyst system. A modified version of *Knölker's* catalyst (**18**) was used in combination with a chiral phosphine ligand (**24**) for the hydrogenation of acetophenone (Figure 1.8), resulting in moderate enantiomeric excess of up to 33% ee [50]. Similarly, the combination of complex (**18**) with chiral Brønsted acids allowed enantioselective hydrogenation reactions of imines to amines [51]. The imine-based iron pincer complex **25** contains two centers of chirality in the pincer backbone and is a catalyst for the enantioselective transfer hydrogenation of ketones and imines. Under the reported conditions, the preparation of *S*-1-phenylethanol with an enantioselectivity of 80% ee from acetophenone was achieved [11b]. The activation of the pre-catalyst presumably involves reduction of the imine function and formation of the same type of active species like with **21** and **23**.

A chiral analog of catalyst **20** has been reported with centers of chirality at the two terminal phosphorus atoms of the pincer ligand in **26**, which allowed for the hydrogenation of acetophenone with moderate enantioselectivity of 48%
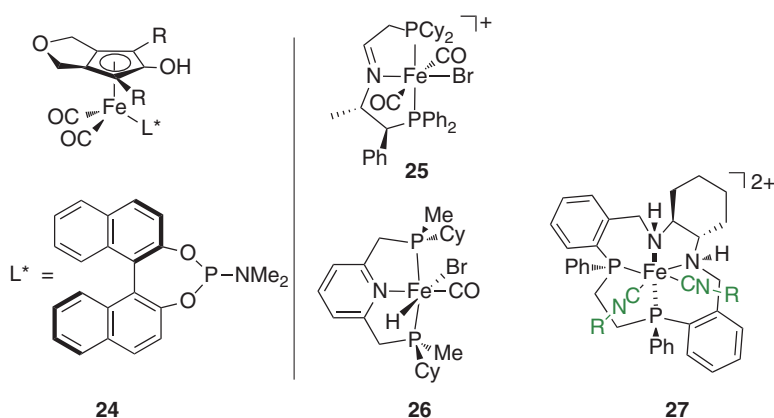
Figure 1.8 Examples of chiral iron catalysts for the enantioselective hydrogenation of ketones. Asterisk indicates a chiral ligand.

ee to *S*-1-phenylethanol [52]. The tetra dentate ligand in complex **27** is similar to the one in complex **19**, but is macrocyclic. Therefore, the macrocyclic ligand provides more rigidity, which in turn increases the stereoselectivity (up to 98% ee for acetophenone hydrogenation) [53].

1.5.2 Hydrogenation of Esters

Some of the iron catalysts for ketone hydrogenation turned out to be active catalysts for the hydrogenation of esters to alcohols (Scheme 1.7). In contrast to the hydrogenation of ketones and aldehydes, two hydrogen transfer steps are required to obtain a mixture of alcohols as products of an ester hydrogenation. After the transfer of the first equivalent of H_2 to the ester, the corresponding hemi-acetal is formed, which is known to be in equilibrium with the corresponding aldehyde and an alcohol. The rapid hydrogenation of the aldehyde intermediate results in the formation of the final products. Notably, for symmetric esters, only one type of alcohol is obtained (e.g. ethanol is obtained for the hydrogenation of ethyl acetate), whereas the hydrogenation of asymmetric esters results in two alcohols (e.g. the hydrogenation of benzyl acetate results in benzyl alcohol and ethanol as products).
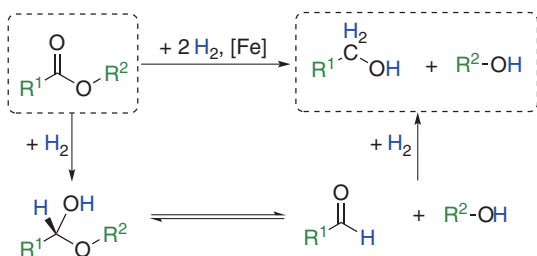

Scheme 1.7 Hydrogenation of esters to alcohols.

The aforementioned amine- and pyridine-based iron pincer complexes were reported to be active catalysts for the hydrogenation of different types of esters. While the pyridine-based iron pincer complex **20** showed significant activity in the hydrogenation of activated trifluoroacetates [38], the amine-based complexes **21** and **23** are capable of hydrogenating nonactivated alkyl- and aryl esters with high productivity and activity [45].

1.5.3 Hydrogenation of Amides

The catalytic hydrogenation of amides can, in principle, lead to different reaction products, depending on the preferred reaction pathway of the hemi-aminal, which is formed as an intermediate of the reaction. The latter is formed after transfer of one equivalent of hydrogen to the amide substrate (Scheme 1.8). Formation of the aldehyde and amine from the hemi-aminal, followed by further reduction of the aldehyde, leads to primary alcohols and amines as major reaction products. Alternatively, the hemi-aminal can eliminate one equivalent of water to give the corresponding imine. The reduction of the latter yields secondary amines (tertiary amines in the case of secondary amides) as major reaction products. The desired formation of alcohols and amines is observed with some of the ruthenium catalysts [33b].
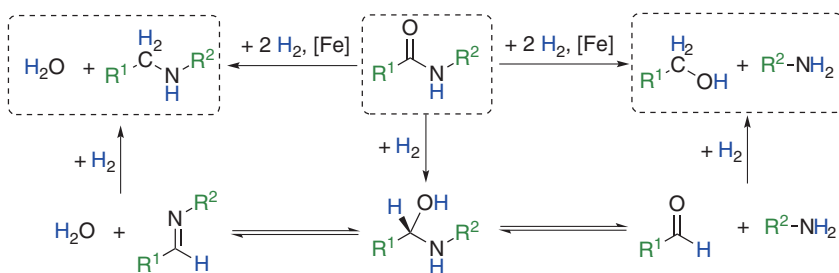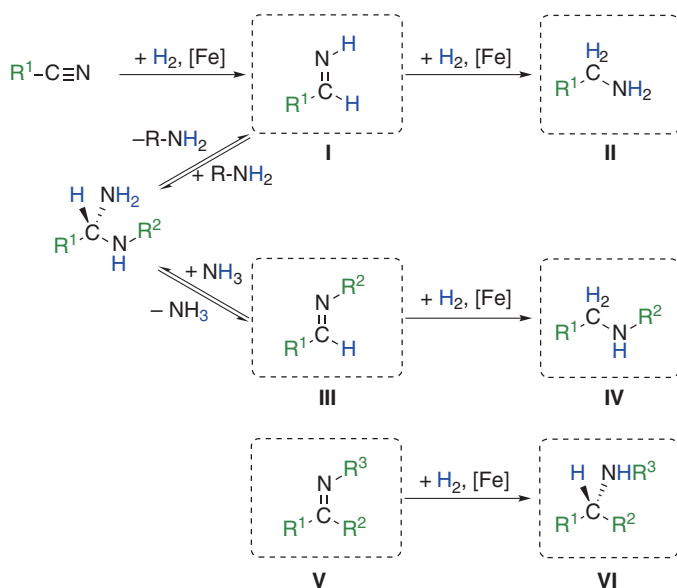

Scheme 1.8 Reaction pathways for the hydrogenation of amides.

Reports about iron-based catalysts for this challenging transformation are rare and usually limited to amine- and pyridine-based iron pincer-type complexes [11a, 40, 46]. So far, all the reported iron catalysts yielded a mixture of alcohol and amine (right pathway in Scheme 1.8). However, the substrate scope for this reaction remains limited, with good catalytic activities for activated and aryl amides but low activities for other substrates. An accelerating effect has been demonstrated for Lewis acid co-catalysts such as formamides [46a], which results in significantly increased activities (TOF) and productivities (TON), as well as a widely applicable protocol.

1.6 Iron-Catalyzed Hydrogenation of C—N Multiple Bonds

Nitriles can be directly hydrogenated to primary amines using iron catalysts. In this two-step process, a primary aldimine (**I**) is generated as an intermediate

Scheme 1.9 Possible reaction products for the hydrogenation of nitriles and imines.

after the first transfer of dihydrogen, which is further hydrogenated to the corresponding primary amine in the second hydrogenation step (Scheme 1.9). More stable and isolable secondary ketimines (**V**) can be hydrogenated as well using iron catalysts, which in the case of prochiral ketimines yields chiral secondary amines (**VI**), valuable products in the value adding chain of the chemical industry.

The hydrogenation of nitriles with an iron-based catalyst has only recently been reported [54]. Similar to the hydrogenation of C-O double bonds, the bifunctional catalysts, such as **23** [54a], **28** [54b], and **29** [54c, d], have been utilized (Figure 1.8). Mechanistic investigations indicate that a concerted proton–hydride transfer takes place in both hydrogenation steps.

In the presence of a primary amine, the initially formed primary aldimine intermediate **I** can be trapped by formation of the corresponding hemi-aminal and gradual NH_3 elimination. The hydrogenation of the resulting secondary aldimine (**III**) yields secondary amines (**IV**). Using complex **25** as catalyst, the scavenging primary amine can be *in situ* generated by complete hydrogenation of the nitrile or it is added to the reaction mixture (Figure 1.9).

The hydrogenation of ketimines (**V**) is of particular interest, as with different substituents R^1 and R^2 the ketimine is prochiral and the hydrogenation of the latter results in chiral amines. Such an enantioselective hydrogenation of ketimines is, for example, an important step in the synthesis of (S)-Metolachlor, one of the most common herbicides, for which iridium catalysts are preferably used [55].

The reactivity of the ketimine substrate strongly depends on the nitrogen-bound substituent R^3 and most publications on iron-based imine hydrogenation
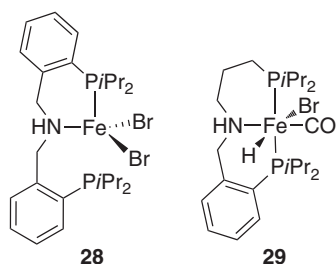
Figure 1.9 Iron-based catalysts for the hydrogenation of nitriles.

catalysts demonstrate catalytic activity for *N*-diphenylphosphinoyl-imines (R³ = P(O)Ph₂). Among the most active and selective iron catalysts for this reaction is complex **22** [42b, 49, 56], but complex **25** and chiral variants of **18** have also been successfully applied as catalysts in the asymmetric hydrogenation of imines [51].

1.7 Conclusion

A major focus of research in homogeneous catalysis in the past decade was on the replacement of noble metal catalysts by their 3d metal counterparts. Among the catalytic reactions, hydrogenation reactions have received considerable attention due to the importance of these atom economic and industrially important transformations. The rapid development in terms of activity, productivity, and selectivity, as well as the fact that nature uses preferably 3d metals in highly active metalloenzymes, may allow predicting that 3d metal based catalyst systems exhibit the potential to one day be real low cost, sustainable, and environmentally benign alternatives for established noble metal based hydrogenation protocols. In this context, iron is a highly attractive metal due to high abundance, low price, and toxicity. A shared characteristic of the most active iron-based catalysts for the hydrogenation of polar substrates is the presence of a tri- or tetra dentate, cooperative ligand in an iron(II) complex. For the hydrogenation of nonpolar substrates, on the other hand, a variety of different catalyst types were reported to be active hydrogenation catalysts. The majority of well-defined catalysts contains a central iron atom with formal oxidation state +2, while only few iron(0) complexes are among the reported catalyst systems.

Understanding the catalytic mechanisms of these reactions is often challenging. This is in part due to analytic limitations on the one hand, and quantum chemical challenges on the other hand, both affiliated with energetically accessible spin states. However, clear trends in reactivity can be observed for different types of catalysts and comprehensive mechanistic investigations will most probably be the basis for designing novel, highly efficient catalytic protocols. A key to the development of highly efficient Fe-based hydrogenation catalysis lies in the suppression of decomposition pathways of iron-based hydrogenation catalysts. Overcoming this challenge will allow to domesticate iron and use its full catalytic potential.

Abbreviations

t-Bu	*tert*-butyl
Cy	cyclohexyl
DFT	density functional theory
dppe	1,2-bis(diphenylphosphino)ethane
ee	enantiomeric excess
hmds	hexamethyldisilazanide
HOMO	highest occupied molecular orbital
LCAO	linear combination of atomic orbitals
LUMO	lowest unoccupied molecular orbital
Me	methyl
$^{i\mathrm{Pr}}$PDI	2,6-di-*iso*-propylphenyl-substituted bis(imino)pyridine
PNP	pincer-type ligand in which the PNP indicates the ligating atoms
Ph	phenyl
PP_3	$P(CH_2CH_2PPh_2)_3$
i-Pr	*iso*-propyl
TOF	turnover frequency
TON	turnover number

References

1 R. Shannon, *Acta Cryst. Sect. A* 1976, 32, 751–767.

2 R.J. Ryther, E. Weitz, *J. Phys. Chem.* 1991, 95, 9841–9852.

3 W. Zuo, A.J. Lough, Y.F. Li, R.H. Morris, *Science* 2013, 342, 1080–1083.

4 S. Chakraborty, P.O. Lagaditis, M. Förster, E.A. Bielinski, N. Hazari, M.C. Holthausen, W.D. Jones, S. Schneider, *ACS Catal.* 2014, 4, 3994–4003.

5 (a) P. Stoppioni, F. Mani, L. Sacconi, *Inorg. Chim. Acta* 1974, 11, 227–230; (b) C. Federsel, A. Boddien, R. Jackstell, R. Jennerjahn, P.J. Dyson, R. Scopelliti, G. Laurenczy, M. Beller, *Angew. Chem. Int. Ed.* 2010, 49, 9777–9780.

6 (a) C.P. Casey, H. Guan, *J. Am. Chem. Soc.* 2009, 131, 2499–2507; (b) C.P. Casey, H. Guan, *J. Am. Chem. Soc.* 2007, 129, 5816–5817.

7 (a) R. Langer, M. A. Iron, L. Konstantinovski, Y. Diskin-Posner, G. Leitus, Y. Ben-David, D. Milstein, *Chem. Eur. J.* 2012, 18, 7196–7209; (b) R. Langer, G. Leitus, Y. Ben-David, D. Milstein, *Angew. Chem. Int. Ed.* 2011, 50, 2120–2124.

8 (a) P.L. Holland, *Acc. Chem. Res.* 2015, 48, 1696–1702; (b) D. Schröder, S. Shaik, H. Schwarz, *Acc. Chem. Res.* 2000, 33, 139–145.

9 E.S. Wiedner, M.B. Chambers, C.L. Pitman, R.M. Bullock, A.J.M. Miller, A.M. Appel, *Chem. Rev.* 2016, 116, 8655–8692.

10 (a) K. Abdur-Rashid, T.P. Fong, B. Greaves, D.G. Gusev, J.G. Hinman, S.E. Landau, A.J. Lough, R.H. Morris, *J. Am. Chem. Soc.* 2000, 122, 9155–9171; (b) R.H. Morris, *J. Am. Chem. Soc.* 2014, 136, 1948–1959.

11 (a) F. Schneck, M. Assmann, M. Balmer, K. Harms, R. Langer, *Organometallics* 2016, 35, 1931–1943; (b) P.O. Lagaditis, P.E. Sues, J.F.

Sonnenberg, K.Y. Wan, A.J. Lough, R.H. Morris, *J. Am. Chem. Soc.* 2014, 136, 1367–1380.

12 J.F. Sonnenberg, N. Coombs, P.A. Dube, R.H. Morris, *J. Am. Chem. Soc.* 2012, 134, 5893–5899.

13 C. Bianchini, A. Meli, M. Peruzzini, P. Frediani, C. Bohanna, M.A. Esteruelas, L.A. Oro, *Organometallics* 1992, 11, 138–145.

14 L.A. Oro, D. Carmona, Rhodium. In: *The Handbook of Homogeneous Hydrogenation* (eds. J.G. de Vries and C.J. Elsevier). Wiley-VCH Verlag GmbH, 2008, 2–30.

15 (a) A.I. Olivos Suarez, V. Lyaskovskyy, J.N.H. Reek, J.I. van der Vlugt, B. de Bruin, *Angew. Chem. Int. Ed.* 2013, 52, 12510–12529; (b) W.I. Dzik, J.I. van der Vlugt, J.N.H. Reek, B. de Bruin, *Angew. Chem. Int. Ed.* 2011, 50, 3356–3358; (c) V. Lyaskovskyy, B. de Bruin, *ACS Catal.* 2012, 2, 270–279.

16 (a) S.C. Bart, E. Lobkovsky, P.J. Chirik, *J. Am. Chem. Soc.* 2004, 126, 13794–13807; (b) S.K. Russell, C. Milsmann, E. Lobkovsky, T. Weyhermüller, P.J. Chirik, *Inorg. Chem.* 2011, 50, 3159–3169; (c) P.J. Chirik, K. Wieghardt, *Science* 2010, 327, 794–795; (d) M.W. Bouwkamp, A.C. Bowman, E. Lobkovsky, P.J. Chirik, *J. Am. Chem. Soc.* 2006, 128, 13340–13341.

17 R.J. Trovitch, E. Lobkovsky, E. Bill, P.J. Chirik, *Organometallics* 2008, 27, 1470–1478.

18 T.N. Gieshoff, M. Villa, A. Welther, M. Plois, U. Chakraborty, R. Wolf, A. Jacobi von Wangelin, *Green Chem.* 2015, 17, 1408–1413.

19 P. Buschelberger, D. Gartner, E. Reyes-Rodriguez, F. Kreyenschmidt, K. Koszinowski, A. Jacobi von Wangelin, R. Wolf, *Chem. Eur. J.* 2017, 23, 3139–3151.

20 (a) R. Noyori, T. Ohkuma, *Angew. Chem. Int. Ed.* 2001, 40, 40–73; (b) S.E. Clapham, A. Hadzovic, R.H. Morris, *Coord. Chem. Rev.* 2004, 248, 2201–2237.

21 (a) C. Gunanathan, D. Milstein, *Science* 2013, 341, 1229712; (b) C. Gunanathan, D. Milstein, *Acc. Chem. Res.* 2011, 44, 588–602; (c) S. Chakraborty, H. Guan, *Dalton Trans.* 2010, 39, 7427–7436; (d) C. Gunanathan, D. Milstein, *Top. Organomet. Chem.* 2011, 37, 55–84; (e) H. Grützmacher, *Angew. Chem. Int. Ed.* 2008, 47, 1814–1818. (f) J.R. Khusnutdinova, M. David, *Angew. Chem. Int. Ed.* 2015, 54, 12236–12273; (g) D. Milstein, *Top. Catal.* 2010, 53, 915–923.

22 (a) P.A. Dub, J.C. Gordon, *ACS Catal.* 2017, 7, 6635–6655; (b) P.A. Dub, N.J. Henson, R.L. Martin, J.C. Gordon, *J. Am. Chem. Soc.* 2014, 136, 3505–3521; (c) P.A. Dub, T. Ikariya, *J. Am. Chem. Soc.* 2013, 135, 2604–2619.

23 W.-H. Wang, Y. Himeda, J.T. Muckerman, G.F. Manbeck, E. Fujita, *Chem. Rev.* 2015, 115, 12936–12973.

24 (a) S. Wesselbaum, V. Moha, M. Meuresch, S. Brosinski, K. M. Thenert, J. Kothe, T. V. Stein, U. Englert, M. Holscher, J. Klankermayer, W. Leitner, *Chem. Sci.* 2015, 6, 693–704; (b) S. Wesselbaum, T. vom Stein, J. Klankermayer, W. Leitner, *Angew. Chem. Int. Ed.* 2012, 51, 7499–7502.

25 R. Xu, S. Chakraborty, S.M. Bellows, H. Yuan, T.R. Cundari, W.D. Jones, *ACS Catalysis* 2016, 6, 2127–2135.

26 J. Neumann, C. Bornschein, H. Jiao, K. Junge, M. Beller, *Eur. J. Org. Chem.* 2015, 2015, 5944–5948.

27 C. Gunanathan, M. Hölscher, W. Leitner, *Eur. J. Inorg. Chem.* 2011, 2011, 3381–3386.

28 J.C. Ott, C.K. Blasius, H. Wadepohl, L.H. Gade, *Inorg. Chem.* 2018, 57, 3183–3191.

29 H. Fong, M.E. Moret, Y. Lee, J.C. Peters, *Organometallics* 2013, 32, 3053–3062.

30 G. Wienhofer, F.A. Westerhaus, R. V. Jagadeesh, K. Junge, H. Junge, M. Beller, *Chem. Commun.* 2012, 48, 4827–4829.

31 D. Srimani, Y. Diskin-Posner, Y. Ben-David, D. Milstein, *Angew. Chem. Int. Ed.* 2013, 52, 14131–14134.

32 (a) E. Balaraman, C. Gunanathan, J. Zhang, L.J.W. Shimon, D. Milstein, *Nat. Chem.* 2011, 3, 609–614; (b) E. Balaraman, Y. Ben-David, D. Milstein, *Angew. Chem. Int. Ed.* 2011, 50, 11702–11705.

33 (a) E. Balaraman, D. Milstein, *Top. Organomet. Chem.* 2014, 48, 19–43; (b) P.A. Dub, T. Ikariya, *ACS Catal.* 2012, 2, 1718–1741.

34 A. Quintard, J. Rodriguez, *Angew. Chem. Int. Ed.* 2014, 53, 4044–4055.

35 R.M. Bullock, *Science* 2013, 342, 1054–1055.

36 T. Zell, D. Milstein, *Acc. Chem. Res.* 2015, 48, 1979–1994.

37 T. Zell, Y. Ben-David, D. Milstein, *Catal. Sci. Technol.* 2015, 5, 822–826.

38 T. Zell, Y. Ben-David, D. Milstein, *Angew. Chem. Int. Ed.* 2014, 53, 4685–4689.

39 J.A. Garg, S. Chakraborty, Y. Ben-David, D. Milstein, *Chem. Commun.* 2016, 52, 5285–5288.

40 T. Zell, B. Butschke, Y. Ben-David, D. Milstein, *Chem. Eur. J.* 2013, 19, 8068–8072.

41 (a) S. Chakraborty, P. Bhattacharya, H. Dai, H. Guan, *Acc. Chem. Res.* 2015, 48, 1995–2003; (b) R.H. Morris, *Acc. Chem. Res.* 2015, 48, 1494–1502.

42 E.A. Bielinski, P.O. Lagaditis, Y. Zhang, B.Q. Mercado, C. Würtele, W.H. Bernskoetter, N. Hazari, S. Schneider, *J. Am. Chem. Soc.* 2014, 136, 10234–10237.

43 E. Alberico, P. Sponholz, C. Cordes, M. Nielsen, H.J. Drexler, W. Baumann, H. Junge, M. Beller, *Angew. Chem.* 2013, 52, 14162–14166.

44 J.F. Sonnenberg, A.J. Lough, R.H. Morris, *Organometallics* 2014, 33, 6452–6465.

45 (a) S. Werkmeister, K. Junge, B. Wendt, E. Alberico, H. Jiao, W. Baumann, H. Junge, F. Gallou, M. Beller, *Angew. Chem. Int. Ed.* 2014, 53, 8722–8726; (b) S. Chakraborty, H. Dai, P. Bhattacharya, N.T. Fairweather, M.S. Gibson, J.A. Krause, H. Guan, *J. Am. Chem. Soc.* 2014, 136, 7869–7872.

46 (a) N.M. Rezayee, D.C. Samblanet, M.S. Sanford, *ACS Catal.* 2016, 6, 6377–6383; (b) U. Jayarathne, Y. Zhang, N. Hazari, W.H. Bernskoetter, *Organometallics* 2017, 36, 409–416.

47 S. Chakraborty, W.W. Brennessel, W.D. Jones, *J. Am. Chem. Soc.* 2014, 136, 8564–8567.

48 (a) C. Sui-Seng, F.N. Haque, A. Hadzovic, A.-M. Pütz, V. Reuss, N. Meyer, A.J. Lough, M. Zimmer-De Iuliis, R.H. Morris, *Inorg. Chem.* 2009, 48, 735–743; (b) C. Sui-Seng, F. Freutel, A.J. Lough, R.H. Morris, *Angew. Chem. Int. Ed.* 2008, 47, 940–943.

49 W. Zuo, S. Tauer, D.E. Prokopchuk, R.H. Morris, *Organometallics* 2014, 33, 5791–5801.

50 A. Berkessel, S. Reichau, A. von der Höh, N. Leconte, J.R.-M. Neudörfl, *Organometallics* 2011, 30, 3880–3887.

51 S. Zhou, S. Fleischer, K. Junge, M. Beller, *Angew. Chem. Int. Ed.* 2011, 50, 5120–5124.

52 R. Huber, A. Passera, A. Mezzetti, *Organometallics* 2018, 37, 396–405.

53 B. Raphael, H. Raffael, M. Antonio, *Angew. Chem. Int. Ed.* 2015, 54, 5171–5174.

54 (a) C. Bornschein, S. Werkmeister, B. Wendt, H. Jiao, E. Alberico, W. Baumann, H. Junge, K. Junge, M. Beller, *Nat. Commun.* 2014, 5, 4111; (b) S. Chakraborty, G. Leitus, D. Milstein, *Chem. Commun.* 2016, 52, 1812–1815; (c) S. Chakraborty, G. Leitus, D. Milstein, *Angew. Chem. Int. Ed.* 2017, 56, 2074–2078; (d) S. Chakraborty, D. Milstein, *ACS Catal.* 2017, 7, 3968–3972; (e) S. Lange, S. Elangovan, C. Cordes, A. Spannenberg, H. Jiao, H. Junge, S. Bachmann, M. Scalone, C. Topf, K. Junge, M. Beller, *Catal. Sci. Technol.* 2016, 6, 4768–4772.

55 H.-U. Blaser, B. Pugin, F. Spindler, M. Thommen, *Acc. Chem. Res.* 2007, 40, 1240–1250.

56 D.E. Prokopchuk, S.A.M. Smith, R.H. Morris, Ligands for iron-based homogeneous catalysts for the asymmetric hydrogenation of ketones and imines. In: *Ligand Design in Metal Chemistry* (eds. M. Stradiotto and R.J. Lundgren) Wiley, 2016, 205–236.